Selection of Image Parameters as the First Step Towards Creating a CBIR System for the Solar Dynamics Observatory

Juan M. Banda
Montana State University
Bozeman, MT. USA
juan.banda@cs.montana.edu

Rafal A. Angryk
Montana State University
Bozeman, MT. USA
angryk@cs.montana.edu

Abstract

This work describes the attribute evaluation sections of the ambitious goal of creating a large-scale content-based image retrieval (CBIR) system for solar phenomena in NASA images from the Solar Dynamics Observatory mission. This mission, with its Atmospheric Imaging Assembly (AIA), is generating eight 4096 pixels x 4096 pixels images every 10 seconds, leading to a data transmission rate of approximately 700 Gigabytes per day from only the AIA component (the entire mission is expected to be sending about 1.5 Terabytes of data per day, for a minimum of 5 years). We investigate unsupervised and supervised methods of selecting image parameters and their importance from the perspective of distinguishing between different types of solar phenomena by using correlation analysis, and three supervised attribute evaluation methods. By selecting the most relevant image parameters (out of the twelve tested) we expect to be able to save 540 Megabytes per day of storage costs for each parameter that we remove. In addition, we also applied several image filtering algorithms on these images in order to investigate the enhancement of our classification results. We confirm our experimental results by running multiple classifiers for comparative analysis on the selected image parameters and filters.

1. Introduction

Our motivation behind this work is based on the large amounts of data that the SDO mission is transmitting, since hand labeling of these images will be an impossible task. There have been several successful CBIR systems for medical images [9], and other domains [7], however, none of them have dealt with the volume of data that the SDO mission generates.

We decided to take a systematic approach to our work and start with the creation of a benchmark image data set that includes multiple types of solar phenomena, all in a balanced distribution, introduced in [29]. Many of the benchmarks published in the solar physics community reflect interests of individual physicists, who tend to specialize in one type of phenomena. Our main difference between the expected SDO data and our benchmark is that our images come from the TRACE mission and are "Partial Sun", which means they represent a particular region of the sun. The SDO images are "Full Disk", meaning they will show the entire sun.

Since SDO images have a resolution of 4096 x 4096 pixels, we cannot risk extracting the image parameters of the whole image without taking into consideration that the solar phenomenon only occurs in part of the image and the rest of the image data will be very similar to images with no solar activity labeled in our data set as "Quiet Sun". By segmenting our images (8 x 8 grids) we can better identify areas that present solar activity instead of analyzing the whole image. This will also make the recognition process more rotation-resistant.

We extract image parameters for individual grid cells, believing that individual types of solar activity will present different values for them. The majority of our featured image parameters are texture based and were selected based on previous works [1, 15] that showed promising results when applied to solar images. We are also testing other parameters that have been used in previous research [9] on images from other domains. Allowing even a singular redundant image parameter would add unneeded computational overhead when processing images in SDO's pipeline, as unnecessary data storage and retrieval costs in our CBIR repository. The main goal of this work is to determine which image parameters we can safely remove while maintaining a high quality, parameter-based representation of the original solar images.

We decided to start our work on the CBIR system by performing an unsupervised attribute evaluation of the extracted image parameters. Our decision behind using a correlation comparison is based on the premise that we can achieve dimensionality reduction by finding strongly correlated (i.e. redundant) image parameters. The use of statistical analysis seems to be more accepted within the astrophysics community and more popular than heuristics and supervised dimensionality reduction techniques (often used by experts coming from AI-related fields). The correlation based approach was also a starting point for the development of CBIR systems in other domains [9]. To

coincide with these unsupervised approach, we also selected several supervised attribute evaluation methods: *Chi Squared [13]*, *Gain Ratio [19]*, and *Info Gain [13]*. We experimented with these supervised methods in order to verify our findings from the unsupervised correlation analysis we performed.

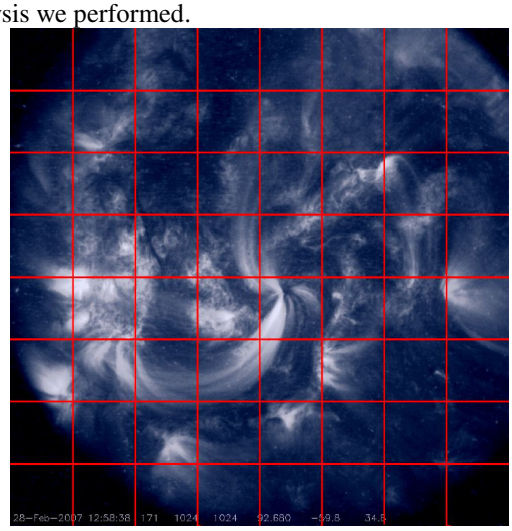

Figure 1. Grid based segmentation applied to our images

The rest of the paper is organized in the following way: A background overview is presented in Sec. 2, in Sec. 3 we give an overview of the steps and experiments we have completed in the process of image parameter selection. We then present our conclusions for the experiments we conducted. Sec. 4 includes the future work we propose to complete in order to have all parts of our CBIR system ready for integration.

2. Background Information

Automatically detecting individual phenomena in solar images has become a popular topic in recent years. Zharkova et al. [28] discuss several methods for identifying features in solar images including artificial neural networks, Bayesian interference, and shape correlation by analyzing five different phenomena: sunspots, inference, plage, coronal mass ejections, and flares. Automatic identification of flares, on the SDO mission, is performed by an algorithm created by Christe et al. [6] which works well for noisy and background affected light curves. This approach will allow detection of simultaneous flares in different active regions. Filament detection for the SDO mission will be provided by the "Advanced Automated Filament Detection and Characterization Code" [2]. The algorithm goes beyond the typical filament identification in that it determines its spine and orientation angle, finds its magnetic chirality (sense of twist), and tracks it from image to image for as long as they are visible on the solar disk. Additionally, if a filament is broken up into two or more pieces it can correctly identify them as a single entity. The coronal jet detection and parameter determination algorithms work on data cubes covering a box enclosing the bright point and extending forward in time. SDO methods for determining the coronal jet parameters are described in detail in [20]. Oscillations on the SDO pipeline are detected using algorithms presented in [8] and [16] that consist of Wavelet transform analysis. In order to detect active regions, the SDO pipeline uses the Spatial Possibilistic Clustering Algorithm (SPoCA). This algorithm produces a segmentation of EUV solar images into classes corresponding to active region, coronal hole, and quiet sun.

As we can see, the majority of the current popular approaches deal with the recognition of individual phenomena and some of them have demanding computational costs. Not until recently, Lamb et al. [15] discussed creating an example-based Image Retrieval System for the TRACE repository. This is the only attempt, which we are aware of, that involves trying to find a variety of phenomena, with the expectation of building a large-scale CBIR system for solar physicists.

2.1. Image Parameters

Based on our literature review, we decided to use some of the most popular image parameters used in investigative analysis of medical images, text recognition, natural scene images and traffic images [4, 5, 9, 10, 12, 14, 17, 18, 24, 27]. From the literature review, we learn that the usefulness of all these image parameters is very domain dependent.

The twelve image parameters that we extracted are presented on table 1. The Gabor Vector [17] was calculated by computing signatures based on Gabor texture filter. This signature is an estimate of the amount of the texture energy that passes through the Gabor filter of a given frequency. In our experiment we used seven different frequencies. We selected our image parameters based on previous work in solar images [1, 15] and other works with monochromatic images [9], but since new image parameters are being published almost every day by image analysis experts, testing everything would be a daunting task. One of our future goals is adding more parameters and verifying what results we would get on our domain specific images.

Table 1. List of Extracted Image Attributes/Parameters

Label	Image parameter [29]
P1	Entropy
P2	Mean
P3	Standard Deviation
P4	3rd Moment (skewness)
P5	4th Moment (kurtosis)
P6	Uniformity

P7	Relative Smoothness (RS)
P8	Fractal Dimension [21]
P9	Tamura Directionality
P10	Tamura Contrast
P11	Tamura Coarseness
P12	Gabor Vector [17]

2.2. Benchmark Dataset

The dataset, first introduced in [29], consists of 1,600 images divided in 8 equally balanced classes representing 8 types of different solar phenomena. All of our images are 1,024 by 1,024 pixels.

Table 2. Benchmark Dataset Characteristics

Event Name	# of images	Wavelength
Active Region	200	1600
Coronal Jet	200	171
Emerging Flux	200	1600
Filament	200	171
Filament Activation	200	171
Filament Eruption	200	171
Flare	200	171
Oscillation	200	171

The benchmark dataset both in its original and pre-processed format is freely available to the public via Montana State University's server [22]. Because of the promising results obtained during preliminary investigations [1] and some earlier works [15], we choose to segment our images for our image parameter extraction.

2.3. Image Filters

The majority of our original TRACE images are not very clear in their unfiltered form. Therefore we decided to apply four computationally inexpensive (F1-F4 in table 3) standard filters to our images in order to make them clearer and hopefully boost our phenomenon classification. We also selected five filters (F5-F9 in table 3) that are highly popular in the image processing community but are considerably more computationally expensive than the first ones we selected. Table 3 shows the list of different filters we applied to our benchmark dataset.

Table 3. Filters Applied to Our Benchmark Dataset

Label	Filter
F1	Contrast with a parameter of 93
F2	Exposure with a parameter of 7.6
F3	Shadow with a parameter of 50%
F4	Threshold with a parameter of 8
F5	4 element Closing operation on an image
F6	3 element Closing operation on an image
F7	4 element Open operation on an image
F8	3 element Open operation on an image
F9	Haar Wavelet Transform

The closing operations performed on filters F5 and F6 dilate and erode the pixel values of the image, filling gaps and maintaining the edges [3]. The open operations performed on filters F7 and F8 are the erosion and dilation of the pixel values of the image, filling gaps and maintaining the edges. They are basically the same as the closing operation but performed in a different order [3]. The Haar Wavelet Transform is commonly used by researchers for image processing purposes [7]. Because it is the simplest wavelet, one would assume that its computational expense would not be critical. Note, we are using one of the coefficients of the wavelet transformed image for extraction of the image parameters selected.

2.4. Unsupervised Attribute Evaluation

Automatic methods for image parameter selection have been proposed in [21, 26]. However, these automatic methods do not directly explain why the selected image parameters are chosen. The method proposed in [9] analyzes correlations between the values of the parameters themselves. Instead of automatically selecting a set of image parameters, it provides the user with information to help them select an appropriate set of image parameters.

To analyze the correlation between different image parameters, we evaluate the correlation between the Euclidean distances $d(q,X)$ obtained for each image parameter of each of the images X from the our benchmark given a query image q. For each pair of query image q and database image X we create a vector $(d_1(q,X), d_2(q,X), \ldots d_m(q,X), \ldots d_M(q,X))$ where $d_m(q,X)$ is the distance of the query image q to the benchmark image X for the $_m$th image parameter, and M is the total number of image parameters. We then calculate the correlation between the d_m over all queries $q = \{q_1, \ldots, q_l, \ldots q_L\}$ and all images $X = \{X_1, \ldots, X_n, \ldots, X_N\}$.

The $M \times M$ covariance matrix, denoted as Σ_{ij} of the d_m is calculated over all N database images and all L query images as:

$$\Sigma_{ij} = \frac{1}{NL} \sum_{n=1}^{N} \sum_{l=1}^{L} (d_i(q_l, X_n) - \mu_i) \cdot d_j(q_l, X_n) - \mu_j) \quad (1)$$

with $$\mu_i = \frac{1}{NL} \sum_{n=1}^{N} \sum_{l=1}^{L} d_i(q_l, X_n) \quad (2)$$

By segmenting each of our images into 64 grid cells, we obtained a number of queries equal to the number of grid cells. Given the covariance matrix Σ_{ij}, we calculate the correlation matrix R as $R_{ij} = \frac{\Sigma_{ij}}{\sqrt{\Sigma_{ii} \Sigma_{jj}}}$ (3)

The entries of this correlation matrix can be interpreted as similarities of different image parameters. A high value R_{ij} means a high similarity between image parameters i and j.

2.5. Supervised Attribute Evaluation

We selected the following supervised attribute evaluation methods.

Chi Squared: This method evaluates the worth of an attribute by computing the value of the chi-squared distribution with respect to the class [13].

Gain Ratio: This method evaluates the worth of an attribute by measuring the gain ratio with respect to the class [19]. This method biases the decision tree against considering attributes with a large number of distinct values. Solving the weakness initially proposed by the *Info gain* method.

Info Gain: This method evaluates the worth of an attribute by measuring the information gain with respect to the class [13].

2.6. Classifiers and Boosting Algorithms

We selected Naïve Bayes (NB) and Support Vector Machines (SVM with a linear kernel) as our linear classifiers and C4.5 as a decision tree classifier. A linear classifier achieves the grouping of items that have similar image parameter values into groups by making a classification decision based on the value of the linear combination of the image parameters.

A decision tree classifier has the goal of creating a model that predicts the class label based on several input variables (i.e. our image parameters). Each interior node corresponds to one of the image parameters. And there are edges to children for the nodes corresponding to each of the possible values of that image parameter. Each leaf represents a value of the target parameter given the values of the image parameters represented by the path from the root to the leaf.

We also incorporated AdaBoost as our boosting algorithm. AdaBoost is short for Adaptive Boosting, the boosting algorithm, is adaptive in the sense that subsequent classifiers built are altered in favor of those instances that were misclassified by previous classifiers.

3. Approach and Experiments

All image parameter extraction, filtering, and supervised and unsupervised attribute evaluation experiments were performed using Matlab R2009b and WEKA 3.6.1.

3.1. Image Parameter Extraction

Here we present the running times of the extraction of the proposed image parameters. Figure 2 presents the time needed to extract our image parameters on 1,600 images, taking into consideration that each image has been segmented in 64 cells. We have a total of 102,400 segments to extract image parameters from.

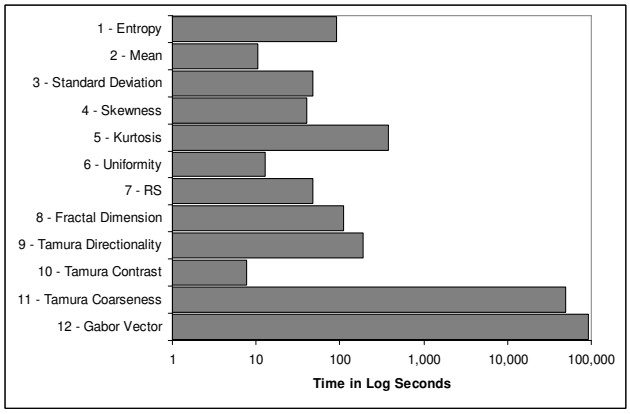

Figure 2. Image Parameter Extraction Times for 1,600 Images.

The reason behind dropping expensive image parameters is that we will have to process data in near real time for the SDO mission, at a rate of eight 4096x4096 images every 10 seconds, so we will have a smaller window than this amount of time to be able to extract all the image parameters that are the most useful and cheapest to calculate.

After analyzing figure1, the Tamura feature coarseness and the Gabor vector were discarded because of their costly computational expense. While the usefulness of these parameters has not been tested, the extreme computational cost of these 2 image parameters makes them immediate candidates to be discarded.

3.2. Image Filters

In order to test the effectiveness and viability of the image filters we selected, we decided to use 2 different criteria: computational expense and classification accuracy. In Figure 3 we show the run times for each filter on our entire 1600 image dataset.

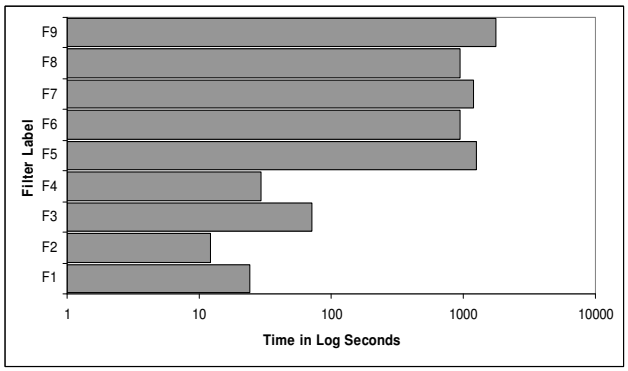

Figure 3. Filtering Time for 1,600 Images.

As we can see from Figure 3 the computationally intensive filters (F5 – F9) take a considerably larger amount of time than the inexpensive ones (F1-F4). However, it almost comes out to 1 second per image for the most expensive, F9 (which is the Haar wavelet). As a

result, we need to verify how much they actually benefit our classification results for the filtered images versus the original images. Table 4 shows the correctly classified instances percentage for our 3 classifiers and the boosted classifier.

Table 4. Classification Accuracy for Filtered Images

	NB	SVM	C4.5	ADA C4.5
Original	31.65%	40.45%	65.60%	**72.41%**
F1	32.83%	40.90%	61.05%	67.10%
F2	30.90%	43.03%	63.58%	69.74%
F3	**35.52%**	**47.61%**	60.43%	67.35%
F4	20.75%	26.13%	40.61%	40.89%
F5	30.63%	34.57%	65.51%	69.82%
F6	30.25%	34.36%	**65.74%**	71.21%
F7	28.38%	38.26%	61.93%	68.07%
F8	28.63%	38.58%	61.37%	68.11%
F9	31.43%	30.91%	60.15%	68.32%

We can see that the highest accuracy percentage was achieved with the original images and the Ada Boost C4.5 classifier. F3 or the Shadow 50% filter provided the best classification results for the Naïve Bayes (NB) and the SVM classifiers. If we decide to use these two classifiers for our CBIR, F3 provides a good improvement over the original image results for a small computational expense. F6 (3 element closing) filter has the overall highest C 4.5 classifier accuracy, but only by 0.14% over the original data. However, F6 had one of the highest computing times; therefore the performance increase is not considerable enough to use this filter for our CBIR system.

Based on these experiments, we can conclude that if we decide to use the C 4.5 and the AdaBoost C 4.5 classifiers in our CBIR system the original non-filtered images provide the best results on the classifiers. If we decide to use Naïve Bayes (NB) or SVM, the linear classifiers, we should consider applying the F3 (Shadow 50%) filter to our images.

3.3. Unsupervised Attribute Evaluation

Using the image parameter evaluation method outlined in section 2.4 for the first scenario we randomly selected a query image from each class and analyzed the correlation between this image and the rest of the same class in order to observe which image parameters are strongly correlated and which ones are not within the same class. In the second scenario, we analyzed the correlation between the query images and the rest of the images of the same wavelength from all other classes in order to observe which image parameters feature higher correlation to the rest of the classes than to the same class. Since Active Regions are some of the most distinguishable classes to discover in our benchmark data set and they are also one of the basic indicators of solar activity occurrence, we decided to present our work by analyzing the correlations between queries of this class.

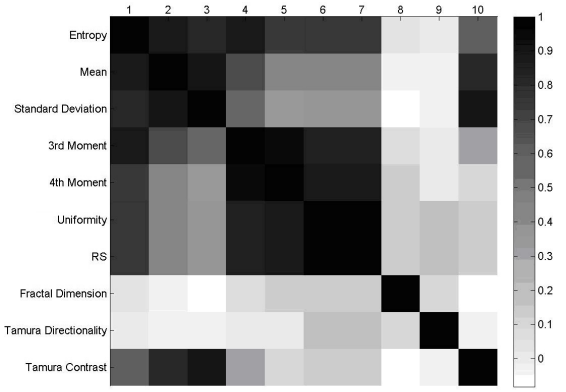

Figure 4: Average correlation map for the Active Region class in the one image as a query against the same class scenario (intra-class correlation).

In Figure 4 we observe a correlation map generated by using one query image of the Active Region class against all the rest of the images within the same class. We can clearly see some image parameters that are weakly correlated against nearly every other parameter, them being: Fractal Dimension and Tamura Directionality. In the strongly correlated section we have: Entropy, 3rd moment and 4th moment with Uniformity and RS, Uniformity with RS and Tamura Contrast with Standard Deviation and Mean.

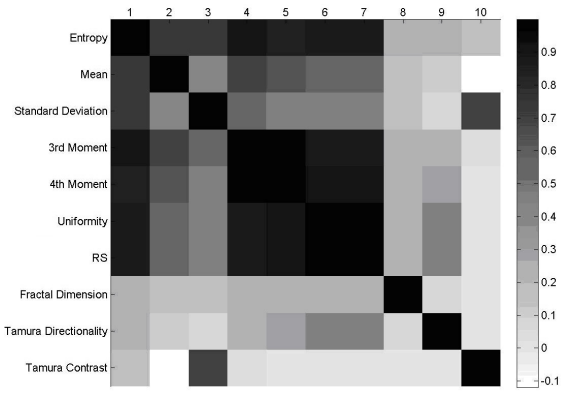

Figure 5: Average correlation map of the Active Region class in the one image as a query against other classes (inter-class correlation) scenario.

Fig. 5 shows the correlation map generated by selecting one query image of the Active Region class and calculating the correlations against all the images for the remaining classes. The weakly correlated parameters are: Tamura Contrast with everything except Standard Deviation, Tamura Directionality with everything, and

Fractal Dimension with everything. These findings are mostly consistent with the correlation analysis of the same class. As for the highly correlated image parameters we have: Entropy, 3rd moment and 4th moment, Uniformity and RS and Tamura Contrast and Standard Deviation. Again, these findings are very consistent with the correlation analysis within the same class.

3.4. Supervised attribute evaluation

For the supervised attribute evaluation we present results from three different methods: *Chi Squared*, *Gain Ratio* and *Info Gain*. Table 6 shows the attribute ranking results for these methods.

Table 6. Attribute Ranking Results

Chi Squared		Info Gain		Gain Ratio	
Rank	**Label**	**Rank**	**Label**	**Rank**	**Label**
13322.43	P1	0.624	P9	0.197	P9
13142.86	P6	0.606	P6	0.166	P1
13104.00	P7	0.605	P7	0.162	P6
11686.84	P9	0.599	P1	0.161	P7
11646.01	P2	0.544	P4	0.157	P10
11504.63	P4	0.532	P5	0.154	P4
11274.94	P10	0.525	P10	0.149	P5
11226.03	P5	0.490	P2	0.137	P2
9040.03	P3	0.398	P3	0.136	P8
6624.91	P8	0.381	P8	0.123	P3

Based on the ranking results we have that on average the top four image parameters are P9, P6, P7, and P1. The bottom four parameters are P8, P3, P2, and P5. After looking at these results and comparing them to our unsupervised method, we see similar grouping of image parameters. Based on these experiments, we can now make educated assumptions as to which parameters whose removal we should experiment with in order to keep our image parameter extraction computational costs to a minimum, while maintaining levels of phenomena recognition comparable to the ones obtained by using all of the parameters.

3.5. Classification results for both supervised and unsupervised attribute evaluations

Utilizing the unsupervised method results, we set up two different scenarios involving the removal of correlated and uncorrelated image parameters. Also, based on the ranking results presented in 3.4, we created seven different experiments that are explained in Table 7. These experiments involve running the selected classifiers and comparing the percentages of accurately classified instances.

Table 7. Description of Experiments.

Label - Experiment Description	
Exp 1	- All Parameters used
Exp 2	- Parameters P8, P9, P10 removed
Exp 3	- Parameters P3, P6, P10 removed
Exp 4	- Parameters P3, P2, P5 removed
Exp 5	- Parameters P9, P6, P1 removed
Exp 6	- Parameters P8, P2, P5 removed
Exp 7	- Parameters P7, P6, P1 removed

Experiments 2 and 3 are based on removing image parameters that are uncorrelated and correlated respectively, according to the unsupervised attribute evaluation we performed (correlation maps). Experiments 4 and 6 are removing the bottom 3 attributes based on their ranking weights in the supervised attribute evaluation experiments. Experiments 5 and 7 remove the top 3 attributes bases on their ranking weights on the supervised attribute evaluation experiments.

Table 8. Classification results obtained for our experiments

	NB	SVM	C45	ADA C45
Exp 1	31.65%	**40.45%**	**65.60%**	**72.41%**
Exp 2	28.59%	34.84%	59.26%	63.86%
Exp 3	**33.23%**	39.50%	63.55%	69.49%
Exp 4	30.17%	34.43%	53.06%	57.38%
Exp 5	30.25%	34.14%	60.17%	64.96%
Exp 6	29.37%	35.58%	56.53%	61.41%
Exp 7	32.72%	37.89%	63.50%	69.32%

From Table 8 we can see that Exp1 (original data), provides us with the best classification results. However, Exp 3 and Exp 7 give us good classification results and considering we removed 3 image parameters (or 30%) this is a very interesting result. The main conclusion we can derive from this comparison is that the more we know about the image parameters and how they are related to each other, the better decision we can make in removing them without suffering a considerable loss in accuracy. We can see that the poor selection of some parameters that are more important in helping the classifiers identify trends in our data can considerably decrease our classification accuracy like in Exp 4 and Exp 6.

4. Future work

In this paper, we have described our first steps towards the goal of building a CBIR system for the SDO mission. The framework that we have created allows us to add any number of new image parameters for experimenting and maybe adding them to the ones we found useful based on this investigation. We can also add other supervised and

unsupervised attribute evaluation methods to further improve our investigations. The analysis of new image filtering algorithms has been also fully automated in our framework, as well as the addition of new classifiers for comparative evaluation.

As with almost all applied research projects on image analysis, our work is not completely extensive since there are too many image parameters, filters, classifiers, out there to try. We selected the ones that, according to our literature review, have shown to produce interesting results in other fields and with similar images to ours. We are open to any suggestions from the scientific community concerning new image parameters, classifiers or attribute evaluation methods to try on our framework.

We are currently looking at multi-dimensional indexing techniques to effectively store the massive amounts of information we expect to receive when SDO generates data at full speed. There is still plenty of work to be done before we have a functional CBIR system.

References

[1] Banda J.M. and Angryk R. "On the effectiveness of fuzzy clustering as a data discretization technique for large-scale classification of solar images.". In Proceedings of the 18th IEEE International Conference on Fuzzy Systems (Jeju Island, Korea, August 2009), pp. 2019-2024

[2] Bernasconi P. N., Rust D. M., and Hakim D. 2005. Advanced Automated Solar Filament Detection And Characterization Code: Description, Performance, And Results. Sol. Phys., (May 2005), 228:97–117.

[3] Burdick H. E. 1997. Digital Imaging: Theory and Applications, McGraw-Hill, 145-150

[4] Cernadas E., Carriön P., Rodriguez P., Muriel E., and Antequera T. 2005. Analyzing magnetic resonance images of Iberian pork loin to predict its sensorial characteristics Comput. Vis. Image Underst. 98, 2 (May. 2005), 345-361. DOI= http://dx.doi.org/10.1016/j.cviu.2004.08.004

[5] Chaudhuri B. B., Nirupam Sarkar. 1995. Texture Segmentation Using Fractal Dimension. IEEE Transactions on Pattern Analysis and Machine Intelligence, vol. 17, no. 1, (Jan. 1995), 72-77, DOI= http://dx.doi.org/10.1109/34.368149

[6] Christe S., Hannah I. G., Krucker S., McTiernan J., and Lin R. P. 2008. RHESSI Microflare Statistics. I. Flare-Finding and Frequency Distributions. ApJ, 677 (April 2008), 1385–1394.

[7] Datta R., Li J and Wang Z. 2005. Content-based Image Retrieval – Approaches and Trends of the New Age. In ACM Intl. Workshop on Multimedia Information Retrieval, ACM Multimedia. (Singapore 2005).

[8] De Moortel I. and McAteer R. T. J. 2004. Waves and wavelets: An automated detection technique for solar oscillations. Sol. Phys. 223 (September 2004), 1–2.

[9] Deselaers T., Keysers D., and Ney H. 2008. Features for Image Retrieval: An Experimental Comparison. Information Retrieval, vol. 11, issue 2, Springer (The Netherlands 03/2008), 77-107.

[10] Devendran V., Hemalatha T., Amitabh W. 2009 SVM Based Hybrid Moment Features for Natural Scene Categorization International Conference on Computational Science and Engineering vol. 1, 356-361

[11] Heliophysics Event Registry [Online] Available: http://www.lmsal.com/~cheung/hpkb/index.html [Accessed: Jan 12, 2010]

[12] Holalu S.S. and Arumugam K. 2006. Breast Tissue Classification Using Statistical Feature Extraction Of Mammograms. Medical Imaging and Information Sciences, Vol. 23 No. 3, 105-107

[13] Kullback, S. and Leibler, R.A. 1951. On Information and Sufficiency. Annals of Mathematical Statistics 22, 79–86.

[14] Kulkarni S., Verma B. 2003. Fuzzy Logic Based Texture Queries for CBIR. Fifth International Conference on Computational Intelligence and Multimedia Applications (ICCIMA'03), 223

[15] Lamb R., 2008. An Information Retrieval System For Images From The Trace Satellite," M.S. thesis, Dept. Comp. Sci., Montana State Univ., Bozeman, MT

[16] McAteer R. T. J., Gallagher P. T., Bloomfield D. S., Williams D. R., Mathioudakis M., and Keenan F. P. 2004. Ultraviolet Oscillations in the Chromosphere of the Quiet Sun. ApJ, 602 (February 2004), 436–445.

[17] Muwei J., Lei L., Feng G. 2009. Texture Image Classification Using Perceptual Texture Features and Gabor Wavelet Features. Asia-Pacific Conference on Information Processing vol. 2, 55-58.

[18] Pentland A.P. (1984) Fractal-based description of natural scenes. IEEE Trans. on Pattern Analysis and Machine Intelligence 6, 661-674

[19] Quinlan J. R. 1986. Induction of decision trees. Machine Learning, 81-106

[20] Savcheva A., Cirtain J., Deluca E. E., Lundquist L. L., Golub L., Weber M., Shimojo M., Shibasaki K., Sakao T., Narukage N., Tsuneta S., and Kano R. 2007. A Study of Polar Jet Parameters Based on Hinode XRT Observations. Publ. Astron. Soc. 59, (Japan November 2007), 771

[21] Schroeder M. 1991. Fractals, Chaos, Power Laws: Minutes from an Infinite Paradise. (W. H. Freeman, New York 1991), 41-45.

[22] SDO Dataset (MSU) [Online], Available: http://www.cs.montana.edu/angryk/SDO/data/ [Accessed: June 10, 2010]

[23] Solar Dynamics Observatory [Online], Available: http://sdo.gsfc.nasa.gov/. [Accessed: June 12, 2010]

[24] Tamura H., Mori S. and Yamawaki T. 1978 Textural Features Corresponding to Visual Perception. IEEE Transaction on Systems, Man, and Cybernetics 8(6), 460–472.

[25] TRACE On-line (TRACE) [Online], Available: http://trace.lmsal.com/. [Accessed: Jan 12, 2010]

[26] Vasconcelos N., Vasconcelos M. 2004. Scalable Discriminant Feature Selection for Image Retrieval and Recognition. In CVPR 2004. (Washington, DC 2004), 770–775.

[27] Wen-lun C., Zhong-ke S., Jian F. 2006. Traffic Image Classification Method Based on Fractal Dimension. IEEE International Conference on Cognitive Informatics Vol. 2. 903-907

[28] Zharkova V., Ipson S., Benkhalil A., and Zharkov S. 2005 Feature recognition in solar images. Artificial Intelligence Review, 23(3), 209–266.

[29] Banda J. M. and Anrgyk R. "An Experimental Evaluation of Popular Image Parameters for Monochromatic Solar Image Categorization". Proceedings of the twenty-third international Florida Artificial Intelligence Research Society conference , Daytona Beach, Florida, USA, May 19–21 2010. pp. 380-385